**Proceedings of the ECCOMAS Thematic International Conference on Simulation and Modeling of Biological Flows (SIMBIO 2011)**
**September 21–23, 2011, VUB, Brussels, Belgium**

# The Development of a Computational, Poroelastic Model of Intestinal Edema

**Jennifer Young**[1] **and Béatrice Rivière**[2]

**1** Computational and Applied Mathematics Department
Rice University
6100 Main St. MS 134, Houston, TX 77005 USA
jjyoung@rice.edu

**2** Computational and Applied Mathematics Department
Rice University
6100 Main St. MS 134, Houston, TX 77005 USA
riviere@rice.edu

## Abstract

Intestinal edema is a medical condition referring to the accumulation of excess fluid in the interstitium of the intestinal wall. To study this phenomenon, we developed a computational, poroelastic model of edema formation in the intestinal wall. The intestinal wall is a multi-layered material, whose individual layers have distinct mechanical properties and structure. Including such details in a numerical model is computationally challenging. We first created and tested several variations of simplified models, where spatial variations in material properties were replaced with average quantities. However, these initial models were not successful at replicating experimental results. This warranted the development of a more complex model that included the layer-to-layer spatial variations in mechanical parameters and capillary concentrations. This detailed model produced results that matched well with the experimental data.
**Keywords:** Edema, Intestine, Poroelasticity, Fluid balance, Discontinuous Galerkin

## Introduction

Under homeostatic conditions, the fluids of the human body are kept at a relatively constant volume by the even exchange of fluids between the circulatory and lymphatic systems [1, 2, 3]. Edema is a medical condition that arises when this balance is disrupted in favor of the excess accumulation of fluid in the interstitium (space between tissue cells) [1, 4]. When this excess build-up of fluid occurs in the intestinal wall, the condition is known as intestinal edema (IE) [5, 6]. IE is known to cause a decrease in intestinal smooth muscle contractility, interfering with the intestine's normal propulsive activities [5, 6, 7]. However the connection between edema and decreased muscle contractility is not clearly understood [6]. Medical personnel have a vested interest in understanding IE since its effects contribute to longer hospital stays and patient recovery time [1, 8].

To assist experimentalists with understanding edema development and its effect on intestinal tissue, a computational model of the phenomenon has been developed. The intestinal wall is a complex structure comprised of several layers with varying mechanical properties. In our model, the intestinal wall is represented as a multi-layered poroelastic medium with an interstitial fluid. We began with several simplified models that utilized average quantities instead of fully modeling the layer-to-layer property variations. However, as the results will show, these models were not able to accurately simulate edema development as observed experimentally in [5]. Consequently, we modified the model to account for the spatially-varying properties of the intestinal wall, and obtained results consistent with experimental data. This final model is quite complex compared to other previous models of the intestine [9, 10, 11]. However, this complexity is necessary for accurately modeling the changes in fluid pressure and volume observed experimentally in edematous tissue.

The organization of the paper is as follows. The biology of the intestine and edema formation will be presented first, followed by a summary of current edema research and previous computational models of the intestine. The mathematical model and numerical methods will be described next. This will be followed by a presentation and interpretation of the simulation results obtained from testing various degrees of complexity of the model. The paper will conclude with an outline of future research goals.

## Biology of Intestinal Edema

The intestine is a tube-shaped organ of the digestive system that extends from the end of the stomach to the rectum [12]. Its main purpose is to absorb nutrients from food passing through the lumen (the intestinal cavity) [13]. Food progresses through the lumen by the coordinated contraction of a layer of smooth muscle cells in the intestinal wall [12]. The muscle layer is supplied by blood and lymphatic systems, as well as a nerve system that stimulates the contraction process [4, 14]. Also part of the intestinal wall is the mucosa and submucosa. The mucosa is the innermost layer and takes up most of the intestinal wall's thickness (about 60-80% [15]). It contains many finger-like projec-

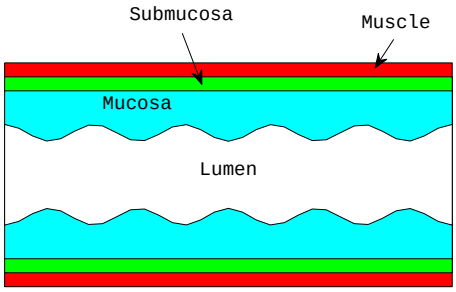


**Figure 1 Diagram of a longitudinal cross-section of the intestine.**

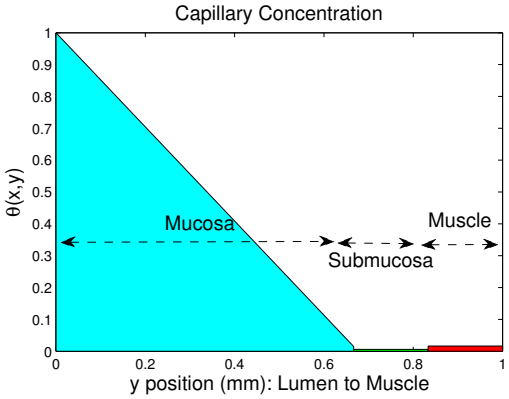


**Figure 2 Capillary concentration $\theta(x, y)$ as one moves vertically up ($y = 0 \rightarrow 1$ mm) through the intestinal layers.**

tions, covered in microvilli that create a large surface area for nutrient absorption [13]. The mucosa has both a blood capillary and lymphatic systems [13], and is the principle area of fluid exchange in the intestinal wall [4]. The mucosa has a Young's modulus on the order of 1 kPa [5]. This is in stark contrast to the 350 kPa Young's modulus of its neighboring layer, the submucosa [6]. The submucosa is thinner (approximately 10-15% of the wall thickness [15]) and contains connective tissue and elastic fibrils. It also houses larger blood and lymph vessels [12]. Figure 1 gives a schematic diagram of the intestinal layers.

In between all the components of the intestinal layers (muscle cells, connective fibers, nerves, vasculature and lymphatics) are the interstitial spaces [2]. The fluid volume of the interstitium is controlled by the hydrostatic and oncotic pressures of the blood and lymph capillaries, and those of the interstitium itself [1, 2, 3]. The circulatory capillaries tend to add fluid to the interstitium, while the lymph capillaries collect the excess fluid and pump it out of the interstitium [1, 2, 3]. This fluid balance can be described mathematically with an ordinary differential equation (ODE):

$$\frac{\partial V}{\partial t} = J_V - J_L \tag{1}$$

where $V$ is the interstitial volume and $J_V$ and $J_L$ are the rates at which fluid is added/removed from the interstitium by the vascular and lymphatic systems, respectively [1]. As mentioned above, these rates are governed by pressure gradients, and are defined here using the microvascular filtration model of Starling-Landis for $J_V$ and the lymph flow model of Drake-Laine for $J_L$ [1]:

$$\begin{aligned} J_V &= K_f\left((P_V - p) - \sigma(\Pi_V - \Pi_{int})\right), \\ J_L &= \frac{1}{R_L}(p + P_p - P_L). \end{aligned}$$

In these equations, $p$ is the interstitial pressure, $P_V$ and $P_L$ are the blood and lymph capillary hydrostatic pressures, $P_p$ is the lymphatic pumping pressure, and $\Pi_V$ and $\Pi_{int}$ are the vascular and interstitial oncotic pressures. Parameters $K_f$, $\sigma$, and $R_L$ are the microvascular filtration coefficient, plasma protein permeability coefficient, and the lymphatic resistance coefficient, respectively. In homeostasis, $J_V$ is equal to $J_L$, and $V$ remains fairly constant, but during edema, $J_V$ is greater than $J_L$ and as a result, $V$ increases.

If one is interested in modeling just the changes in volume in a very local interstitial area of the body, Equation 1 would be sufficient. However, for IE we are interested in edema's effect on the whole intestinal wall. Each of its layers plays a different role in and is affected differently by edema development. For example, there is a higher concentration of blood and lymph capillaries in the mucosa compared to the submucosa or muscle layer. The capillary concentration even varies spatially within the mucosa, with a higher concentration near the lumen. These differences create different rates of fluid exchange and should be taken into account in the computation of $\partial V/\partial t$. This is done in our model by adding a spatially-dependent coefficient $\theta(x, y) \in [0, 1]$ that describes the concentration of capillaries at position $(x, y)$ relative to other positions in the intestine. Equation 1 thus becomes:

$$\frac{\partial V}{\partial t} = \theta(x, y)(J_V - J_L) \tag{2}$$

A plot of $\theta(x, y)$ used in the simulations with non-uniform capillary concentrations, (derived from biological descriptions of blood and lymph capillary locations [4]) is shown in Figure 2.

But volume change is not the only quantity of interest in edema modeling. IE has been linked to decreased intestinal muscle contractility so we are interested in modeling edema's mechanical effects on the intestine for possible explanations of this relationship. This means we want to model and monitor quantities such as interstitial pressure and elastic deformation in the intestinal wall, to understand the stresses and strains placed on each layer. This warrants the replacement of the ODE in Equation 2 with a partial differential equation (PDE) system. A poroelastic model that describes the deformation of the solid phase of the intestine and the evolution of the pressure of the interstitial fluid was chosen, and will be described in the Mathematical Model section.

## Previous Work

A great deal of experimental work on intestinal edema has been conducted by the lab of Cox Jr. et. al. at the Center for Microvascular and Lymphatic Studies at the University of Texas-Houston Medical School. They have carried out experiments that examine: (1) mechanisms of edema formation [16], (2) various treatment methods for edema [5, 7], (3) treatment methods for improving the edema-induced impaired intestinal transit [8], and (4) signaling pathways that may link edema to decreased smooth muscle contractility [17, 18, 19].

Mathematical models of the intestine have previously been developed for simulating various intestinal activities. Robertson-Dunn et. al. represented the intestine as a chain of coupled oscillators and utilized an ODE system to model the slow wave electrical activity in the small intestine [9]. Metry et. al. created a finite element model of the lumen, and utilized the Stokes' equation to model fluid flow and pressure in the intestinal cavity during peristaltic activity [10]. In this work, the intestinal wall was modeled only as an impermeable, fixed boundary of the lumen. Francea et. al. created a virtual three-dimensional model of the intestine based on a central spline skeleton, for surgery training [11]. In these three models, the intestinal wall is considered to be a homogeneous material, where individual properties of the intestinal layers are not considered. For the activities being studied by these models, such an assumption is likely acceptable. However intestinal edema is a complex phenomenon involving fluid flow and elastic deformation within the intestinal wall, and thus requires a more detailed model.

## Mathematical Model

The mathematical model is based on Biot's theory of poroelasticity [20, 21]. The intestine is modeled as an elastic, porous medium whose void spaces are completely filled with interstitial fluid. The system of PDEs is constructed from the conservation of mass and conservation of momentum equations for the fluid and solid phases. The model assumes that the fluid is incompressible and that the fluid-solid boundaries are impermeable. The main equations will now be presented, but details of the model derivation can be found in [22, 23]. The equations that arise from the combination of the fluid and solid conservation of mass equations are:

$$-\frac{k}{\mu}\Delta p + \frac{\partial \epsilon}{\partial t} + \phi(p) = 0,$$
$$\epsilon = \nabla \cdot \mathbf{w}.$$

where $k$ is the permeability coefficient of the solid material, $\mu$ is the fluid viscosity, $p$ is the interstitial fluid pressure, $\mathbf{w}$ is the displacement vector of the solid phase, $\epsilon$ is the divergence of the displacement vector, and $t$ is time. The $\phi(p)$ term is a source term representing any fluid added or removed from the system. This is where the ODE of Equation 2 will come into play, with: $\phi(p) = \theta(x,y)(J_V - J_L)$. Recall that both $J_V$ and $J_L$ involve the interstitial pressure $p$, so this dependence is emphasized in labeling the source term as $\phi(p)$.

To complete our mathematical model, we use a conservation of momentum equation, describing all forces acting on the porous medium. In a comparison of magnitudes, the forces most influential to the system are the pressure forces of the fluid and the elastic forces of the solid. The conservation equation thus takes the form:

$$\nabla \cdot \left[\gamma(p)(\nabla \mathbf{w} + (\nabla \mathbf{w})^T) + \lambda(p)(\nabla \cdot \mathbf{w})\mathbf{I}\right] - \nabla p = 0. \quad (3)$$

where the first part represents the forces from elastic deformation, and the second term is the force from pressure. The tensor $\mathbf{I}$ is the identity matrix and $\gamma(p)$ and $\lambda(p)$ are pressure-dependent material parameters of the solid phase. It has been shown experimentally in intestinal tissue that there is a threshold pressure over which the elastic moduli of the intestinal material decrease [3, 4, 6]. This sudden change is thought to be due to the breaking of connective fibrils within the tissue [3]. This is represented in the model by piecewise constant functions for $\gamma(p)$ and $\lambda(p)$. For example:

$$\gamma(p) = \begin{cases} \gamma_1 & \text{if } p < p_{thres} \\ \gamma_2 & \text{if } p \geq p_{thres} \end{cases}$$

with a similar expression for $\lambda(p)$. As mentioned previously the different layers of the intestine have different mechanical properties, so in the model each layer will have a different value for $\gamma_1$, $\gamma_2$, $\lambda_1$ and $\lambda_2$. Table 1 contains the measured Young's and shear moduli values of the three intestinal layers. The shear modulus is the $\gamma(p)$ parameter in our equation, and the $\lambda(p)$ parameter can be obtained from the Young's modulus (denoted $E(p)$) and shear modulus with: $\lambda(p) = \frac{\gamma(p)(E(p)-2\gamma(p))}{(3\gamma(p)-E(p))}$. Utilizing the substitution $\epsilon = \nabla \cdot \mathbf{w}$ and distributing the divergence operator in Equation 3, the final system of equations utilized in our simulations is: :

$$\frac{\partial \epsilon}{\partial t} = \frac{k}{\mu}\Delta p - \phi(p), \quad (4)$$
$$\nabla \cdot \mathbf{w} = \epsilon, \quad (5)$$
$$-\gamma(p)\Delta \mathbf{w} + \nabla p = (\gamma(p) + \lambda(p))\nabla \epsilon. \quad (6)$$

## Numerical Methods

The domain for this problem is a two-dimensional representation of a longitudinal cross-section of the intestinal wall. Within this domain are three subdomains that represent the mucosa, submucosa and muscle layers. Each layer is discretized with triangular elements. Figure 3 shows the discretized domain in its initial shape. The equations will

**Table 1 Young's and shear moduli of the three intestinal wall layers, obtained from [5, 6, 24, 25].**

| | Mucosa | Submucosa | Muscle |
|---|---|---|---|
| Young's Modulus: $p < p_{thres}$ | 1 kPa | 350 kPa | 40 kPa |
| $p \geq p_{thres}$ | 0.5 kPa | 250 kPa | 20 kPa |
| Shear Modulus: $p < p_{thres}$ | 0.4 kPa | 140 kPa | 16 kPa |
| $p \geq p_{thres}$ | 0.2 kPa | 100 kPa | 8 kPa |

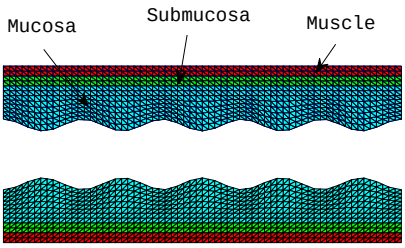


**Figure 3 The discretized domain of a longitudinal cross-section of the intestine.**

be solved on the top half of the domain, and the bottom half will be shown in the results as the top's mirror image.

Equations 4 - 6 are solved numerically with a discontinuous Galerkin finite element (DGFE) method [26], coupled with a forward Euler scheme for time advancement. For simplicity of notation, we will discuss the time discretization first, presenting the equations in the format of 4 - 6. Then the DGFE algorithm will be presented, and we will suppress time step notation.

The time advancement procedure is broken down into a two step process. First, given current values for variables $p$ and $\epsilon$ at time step $m$, Equation 4 is used to compute $\epsilon$ at time step $m+1$ with a forward Euler scheme:

$$\frac{\epsilon^{m+1}-\epsilon^m}{\delta t} = \frac{k}{\mu}\Delta p^m - \phi(p^m) \tag{7}$$

where $\delta t$ is the size of the time step. The updated $\epsilon^{m+1}$ values are then inserted into the right hand sides of Equations 5 and 6, and these two equations are solved for $p^{m+1}$ and $\mathbf{w}^{m+1}$. Values for $\gamma$ and $\lambda$ are based on $p^m$:

$$\nabla \cdot \mathbf{w}^{m+1} = \epsilon^{m+1} \tag{8}$$

$$-\gamma(p^m)\Delta \mathbf{w}^{m+1} + \nabla p^{m+1} = (\gamma(p^m)+\lambda(p^m))\nabla \epsilon^{m+1} \tag{9}$$

Both steps are carried out in a DGFE framework. The main idea behind DGFE is to approximate the solution of a PDE with a piecewise discontinuous polynomial function. Piecewise refers here to finding a separate polynomial solution for each triangular element $T_j$, $j = 1..N$ where $N$ is the total number of elements in the domain. Discontinuous means that two neighboring triangles need not have matching solutions on their common edge. We denote the set of edges in our domain with $\Gamma = \Gamma_I \cup \Gamma_B$, where $\Gamma_I$ are interior edges and $\Gamma_B$ are the boundary edges.

The polynomial approximation on element $T_j$ for a particular problem variable can be written as $\sum_{k=0}^{n} \alpha_k^j \psi_k^j(x,y)$, where $\psi_k^j(x,y)$ are a preselected set of basis functions, and $\alpha_j^k$ are the unknown coefficients. The solution over the whole domain can be written as:

$$P(x,y) = \sum_{j=1}^{N}\sum_{k=0}^{n} \alpha_k^j \Psi_k^j(x,y)$$

where

$$\Psi_k^j(x,y) = \begin{cases} \psi_k^j(x,y) & \text{if } (x,y) \in T_j \\ 0 & \text{if } (x,y) \notin T_j \end{cases}$$

For Equations 4 - 6, there are four unknowns: $p$, $\epsilon$ and $\mathbf{w} = [w_1, w_2]$, where $w_1$ and $w_2$ are the $x$ and $y$ displacements. We will denote their polynomial approximations as: $P_p$, $P_\epsilon$, and $P_\mathbf{w} = [P_{w_1}, P_{w_2}]$ respectively, and utilize these in the equations below. To solve for the coefficients of these polynomial approximations, we multiply Equations 4 - 6 by test functions: $v_p$, $v_\epsilon$, and $\mathbf{v_w}$. These test functions are the same basis functions ($\psi_k^j(x,y)$) of the polynomial approximation for each variable. We then integrate each equation over all elements $T_j$. At this stage, Equations 4 - 6 have become:

Equation 4:

$$\sum_{j=1}^{N}\int_{T_j}\frac{\partial P_\epsilon}{\partial t}v_\epsilon = \sum_{j=1}^{N}\int_{T_j}\left(\nabla\cdot(\frac{k}{\mu}\nabla P_p)\right)v_\epsilon - \sum_{j=1}^{N}\int_{T_j}\phi(P_p)v_\epsilon$$

Equation 5:

$$\sum_{j=1}^{N}\int_{T_j}(\nabla\cdot P_\mathbf{w})v_p = \sum_{j=1}^{N}\int_{T_j}P_\epsilon v_p$$

Equation 6:

$$-\sum_{j=1}^{N}\int_{T_j}(\nabla\cdot(\gamma(P_p)\nabla P_\mathbf{w}))\cdot\mathbf{v_w} + \sum_{j=1}^{N}\int_{T_j}\nabla P_p\cdot\mathbf{v_w} = \sum_{j=1}^{N}\int_{T_j}(\gamma(P_p)+\lambda(P_p))\nabla P_\epsilon\cdot\mathbf{v_w}$$

The next step is to carry out integration by parts on the two Laplace operators in the system. Before doing so, we need to define the *average* and *jump* of a quantity on the edge of an element. Let $e$ be an edge between elements $T_j$ and $T_k$, with $j > k$. The average and jump of quantity $q$ along edge $e$ are denoted respectively as:

$$\{q\} = \frac{1}{2}q|_{T_j^e} + \frac{1}{2}q|_{T_k^e} \qquad [q] = q|_{T_j^e} - q|_{T_k^e}$$

If $e \in \Gamma_B$, and $e$ is an edge of $T_j$ then:

$$\{q\} = [q] = q|_{T_j^e}$$

After integration by parts and an application of Green's theorem, the system looks like:
Equation 4:

$$\sum_{j=1}^{N}\int_{T_j}\frac{\partial P_\epsilon}{\partial t}v_\epsilon = -\frac{k}{\mu}\sum_{j=1}^{N}\int_{T_j}\nabla P_p\cdot\nabla v_\epsilon + \frac{k}{\mu}\sum_{e\in\Gamma}\int_e\{\nabla P_p\}\mathbf{n}_e\cdot[v_\epsilon] - \sum_{j=1}^{N}\int_{T_j}\phi(P_p)v_\epsilon$$

Equation 5:

$$\sum_{j=1}^{N}\int_{T_j}v_p\nabla\cdot P_{\mathbf{w}} = \sum_{j=1}^{N}\int_{T_j}P_\epsilon v_p$$

Equation 6:

$$\sum_{j=1}^{N}\int_{T_j}\gamma(P_p)(\nabla P_{\mathbf{w}}:\nabla\mathbf{v}_{\mathbf{w}}) - \sum_{e\in\Gamma}\int_e\gamma(P_p)\{\nabla P_{\mathbf{w}}\}\mathbf{n}_e\cdot[\mathbf{v}_{\mathbf{w}}] - \sum_{j=1}^{N}\int_{T_j}P_p\nabla\cdot\mathbf{v}_{\mathbf{w}} + \sum_{e\in\Gamma}\int_e\{P_p\}[\mathbf{v}_{\mathbf{w}}]\cdot\mathbf{n}_e = \sum_{j=1}^{N}\int_{T_j}(\gamma(P_p)+\lambda(P_p))\nabla P_\epsilon\cdot\mathbf{v}_{\mathbf{w}}$$

where the normal vector $\mathbf{n}_e$ is assumed to point from element $j$ to $k$. The system in this form is not convergent or stable [26]. To remedy this, we add stabilization and penalty terms. These terms are constructed from jumps of the variables we are trying to solve for. An exact solution of the problem would be a continuous function of each variable $q$, and thus $[q] = 0$. Adding a term with a jump $[q]$ penalizes the approximate solution as it moves away from the exact solution. The complete DGFE system is:
Equation 4:

$$\sum_{j=1}^{N}\int_{T_j}\frac{\partial P_\epsilon}{\partial t}v_\epsilon + \sum_{e\in\Gamma}\frac{\sigma}{|e|}\int_e[P_\epsilon]\cdot[v_\epsilon] = -\frac{k}{\mu}\sum_{j=1}^{N}\int_{T_j}\nabla P_p\cdot\nabla v_\epsilon + \frac{k}{\mu}\sum_{e\in\Gamma}\int_e\{\nabla P_p\}\mathbf{n}_e\cdot[v_\epsilon] + \sum_{e\in\Gamma}\frac{\sigma}{|e|}\int_e[P_p]\cdot[v_\epsilon] + \beta\sum_{e\in\Gamma}\int_e\{\nabla v_\epsilon\}\mathbf{n}_e\cdot[P_p] - \sum_{j=1}^{N}\int_{T_j}\phi(P_p)v_\epsilon$$

Equation 5:

$$\sum_{j=1}^{N}\int_{T_j}v_p\nabla\cdot P_{\mathbf{w}} + \beta\sum_{e\in\Gamma}\int_e\{v_p\}[P_{\mathbf{w}}]\cdot\mathbf{n}_e = \sum_{j=1}^{N}\int_{T_j}P_\epsilon v_p$$

Equation 6:

$$\sum_{j=1}^{N}\int_{T_j}\gamma(P_p)(\nabla P_{\mathbf{w}}:\nabla\mathbf{v}_{\mathbf{w}}) - \sum_{e\in\Gamma}\int_e\gamma(P_p)\{\nabla P_{\mathbf{w}}\}\mathbf{n}_e\cdot[\mathbf{v}_{\mathbf{w}}] + \sum_{e\in\Gamma}\frac{\sigma}{|e|}\int_e[P_{\mathbf{w}}]\cdot[\mathbf{v}_{\mathbf{w}}] - \sum_{j=1}^{N}\int_{T_j}P_p\nabla\cdot\mathbf{v}_{\mathbf{w}} + \beta\sum_{e\in\Gamma}\int_e\{\nabla\mathbf{v}_{\mathbf{w}}\}\mathbf{n}_e\cdot[P_{\mathbf{w}}] + \sum_{e\in\Gamma}\int_e\{P_p\}[\mathbf{v}_{\mathbf{w}}\cdot\mathbf{n}_e = \sum_{j=1}^{N}\int_{T_j}(\gamma(P_p)+\lambda(P_p))\nabla P_\epsilon\cdot\mathbf{v}_{\mathbf{w}}$$

In this system, $\beta, \sigma \in \mathbb{R}$ are the stabilization and penalty coefficients. For the simulations done in this work, $\beta = \sigma = 1$ which corresponds to the nonsymmetric interior penalty Galerkin method [27].

This is the system that is solved in the two step process described above. The coefficients of the approximate polynomial solutions are found by organizing the equations into linear systems. In the first step we solve the first equation for the coefficients of $P_\epsilon$ at time step $m+1$. In the second step, the two remaining equations are combined into a large linear system whose unknowns are the coefficients of $P_p$ and $P_{\mathbf{w}}$ at time step $m+1$. The code for this problem was adapted from [26]. The linear solve in both steps is done utilizing PETSc [28, 29, 30].

## Model Simulations

We know from experimental data that the three main layers of the intestinal wall have distinct mechanical properties, and that there is a non-uniform distribution of blood and lymph capillaries across these layers [4, 5]. Addressing both ideas in a computational model is challenging. The large differences in elasticity moduli and capillary concentrations can create large pressure gradients, forcing the use of smaller time steps and stricter penalty terms to keep the results stable. As we developed the model, we tested various simplifications to see if we could match the experimental results of [5] without fully modeling the two concepts described above. These simplifications included utilizing average Young's and shear moduli for the entire domain and using a uniform capillary concentration in all layers. The results of these tests are presented below, but first we describe the experiments of [5] that we will utilize as a means of comparison.

In these experiments, intestinal edema was induced in a group of Sprague Dawley rats by increasing their blood capillary pressure. There was also a control group whose blood capillary pressure was not raised. After approximately thirty minutes, the interstitial pressure in the submucosa was measured, as well as the overall gain in fluid volume in the intestine. To mimic the edema scenario in our simulations we utilized parameter values from these experiments and from the literature in Equations 4 - 6 (see

[23] for parameter table). In the edema case $P_V$ (blood capillary pressure) was set to an elevated 20 mmHg [5], (when it is normally approximately 12 mmHg [5, 31]). In the experiments, the rats in the edema group had final interstitial pressures of 3.8 $\pm$ 0.34 mmHg in the submucosa, and their intestinal volume increased by approximately 19.8% $\pm$ 5%. We will use these two data points as a means of comparison to our simulation results.

The following variations of the model will now be tested: (1) Average elasticity moduli with a uniform capillary concentration, (2) Average elasticity moduli with a non-uniform capillary concentration, (3) Varying elasticity moduli with a uniform capillary concentration, (4) Varying elasticity moduli with a lower, uniform capillary concentration, (5) Varying elasticity moduli and non-uniform capillary concentration.

For the simulations described below, all variables are initialized to zero. The left and right boundaries of the domain are fixed. The top and bottom boundaries are deformable.

## Average Elasticity Moduli and Uniform Capillary Distribution

The experimentally measured elasticity moduli of the intestinal layers are given in Table 1. Utilizing the width of each layer as a weight, we can compute a weighted average Young's modulus (66 kPa for $p < p_{thres}$ and 44 kPa for $p \geq p_{thres}$) and shear modulus (26 kPa for $p < p_{thres}$ and 18 kPha for $p \geq p_{thres}$) for the whole intestinal wall. The $\theta(x, y)$ function depicted in Figure 2 is a biologically realistic description of the capillary distribution in the intestinal wall. In this first test, we replace this $\theta(x, y)$ with a uniform distribution by integrating: $\Theta = \int_0^1 \theta(x, y)dy$, and utilizing the value obtained for $\Theta$ as the capillary concentration across the whole domain. For this test, $\Theta = \theta(x, y) = 0.3414$. In this simulation, the final average interstitial pressure of the submucosa was 9.2 mmHg and the percent total volume change of the intestinal wall was -10%. These values are very different from the experimental results.

Unlike the experiments, with this model, we are able to track the average pressure and percent volume increase over time, separately in each layer. These results are shown in Figure 4. A contour plot of the interstitial pressure at the end of the simulation is also shown in Figure 4. This contour plot also shows the deformation of the domain. We can see from these plots that initially, the pressure rises similarly in all layers and volume gain is also equal in all layers. At approximately 500 seconds in, the submucosa pressure is in the 4-5 mmHg range (close to experimental observation for edema), but the volume increase is at 3-4% (well below experimental observation). After 500 seconds, the pressures level off for a period and then diverge, and the volume decreases.

## Average Elastic Moduli and Non-Uniform Capillary Distribution

In this second test, we assign the average moduli derived in the first test, to all layers of the intestine, and utilize the biological, spatially-varying $\theta(x, y)$ shown in Figure 2. When this test was run, the simulation was not able to complete all of the time steps due to some variables going to extreme values. The pressure and percent volume increase graphs, and a pressure contour plot of the domain at the end of this simulation are also shown in Figure 4. In this test, all layers have the same mechanical properties but the rate at which fluid is being added varies spatially. Because of this, we immediately see pressure differences arise, with pressure growth in the mucosa and decline in the submucosa and muscle layer. At the point in time when the simulation ends prematurely, the pressure in the submucosa is approximately -2.5 mmHg and the percent volume increase is 3.7%.

## Varying Elasticity Moduli and Uniform Capillary Distribution

In this third test, we utilize the elastic parameters given in Table 1 and a uniform capillary distribution: $\Theta = \theta(x, y) = 0.3414$. As in the second test, this simulation was not able to complete all of the time steps due to extreme values arising in some variables. The pressure values initially grow rapidly in the submucosa, then hit a turning point near 5 mmHg. The average submucosal pressure then takes a sharp dive, down into negative pressure values, ending near -4 mmHg before the computation stops prematurely. The average pressure over time and the percent volume increase in each layer are shown in Figure 5. The percent increase in each layer is fairly uniform, but the overall increase in volume of 5.8% is three times smaller than experimental observation for edema. Figure 5 also shows a pressure contour plot of the domain at the end of this simulation. One can see that the pressure is not uniform within each layer, and pockets of extreme values have formed.

## Varying Elasticity Moduli and Lower Uniform Capillary Distribution

In test number four, we use the biologically-correct elasticity moduli but a smaller capillary concentration across the domain. We utilized $\Theta = \theta(x, y) = 0.0059$, which is the capillary concentration of the submucosa of $\theta(x, y)$ in Figure 2. This simulation was able to run to completion, and we obtain final pressure values for the submucosa of 4.41 mmHg, which is close to the experimentally measured value. However, the volume increase in the intestinal wall for this simulation was 0.65% which is much smaller than what is experimentally observed. The plots of these results are also shown in Figure 5. From the pressure contour plot for this simulation one can see that the domain has hardly deformed.

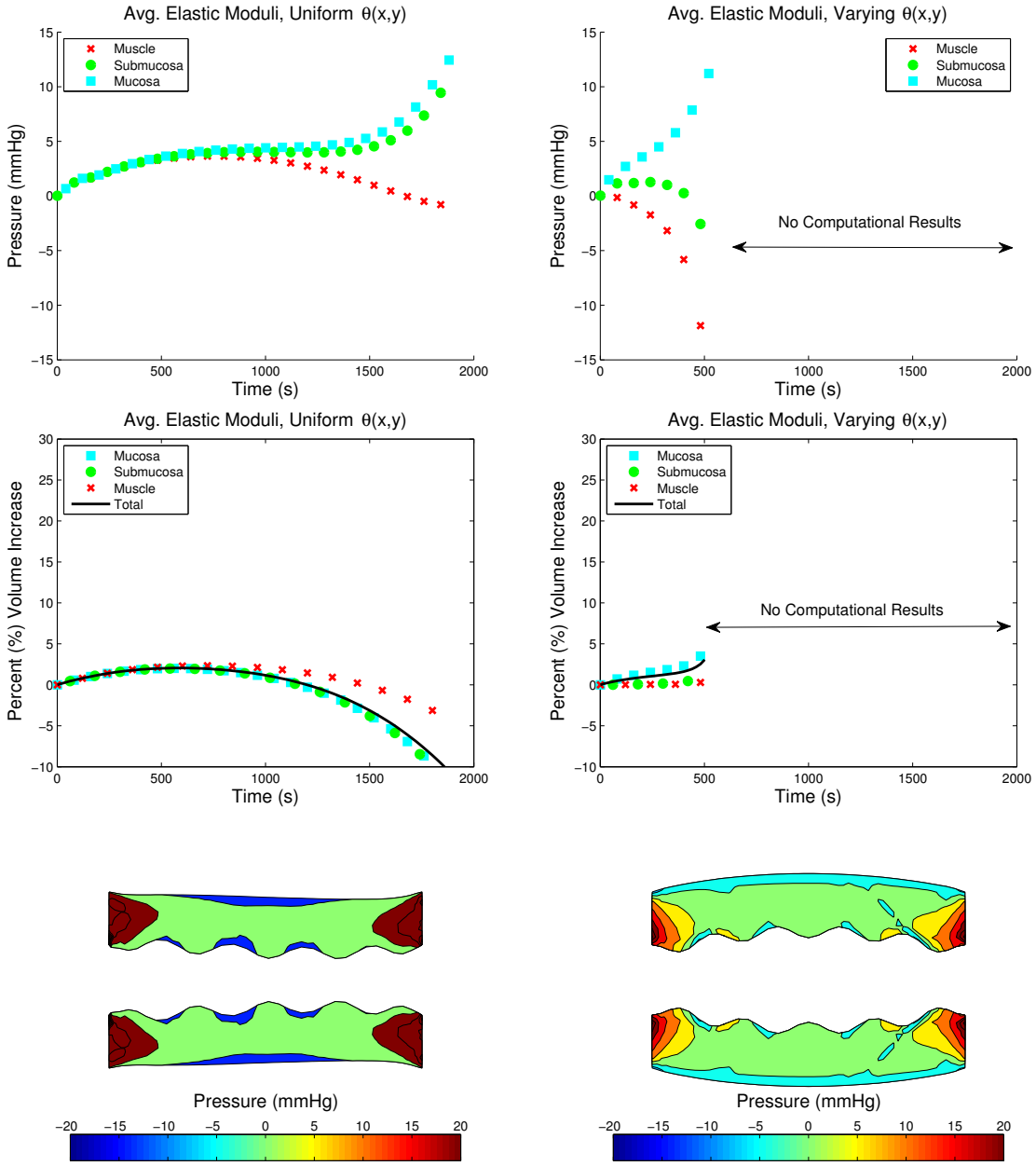


**Figure 4 Top Row: Average interstitial pressure versus time for the three subdomains, for the two average elastic moduli cases. Middle Row: Percent volume increase versus time for the three subdomains and their total, for the two average elastic moduli cases. Bottom Row: Contour plots of the pressure at the end of the two average elastic moduli cases.**

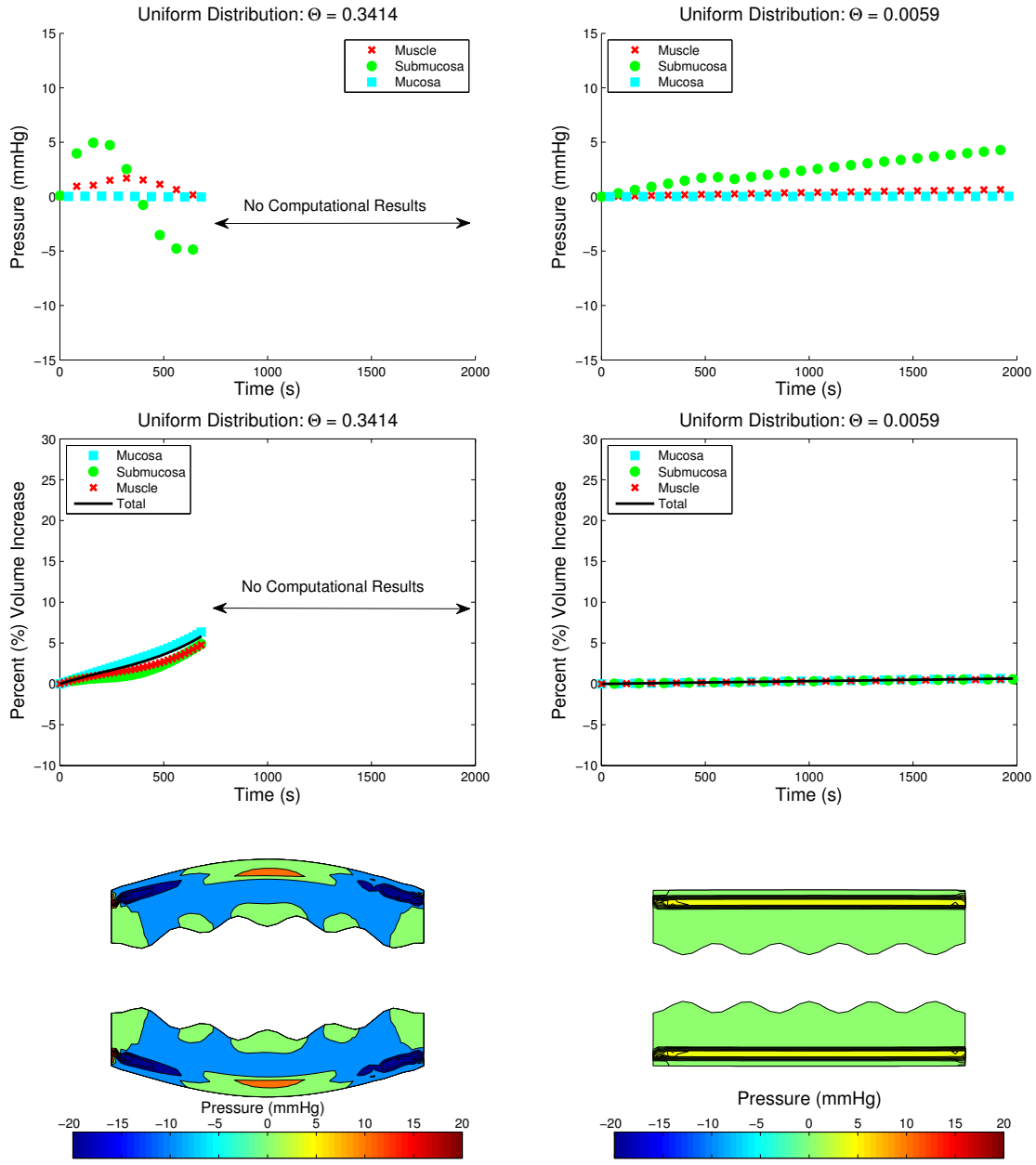


**Figure 5 Top Row: Average interstitial pressure versus time for the three subdomains, for the two uniform capillary distributions cases. Middle Row: Percent volume increase versus time for the three subdomains and their total, for the two uniform capillary distribution cases. Bottom Row: Contour plots of the pressure at the end of the two uniform capillary distribution cases.**

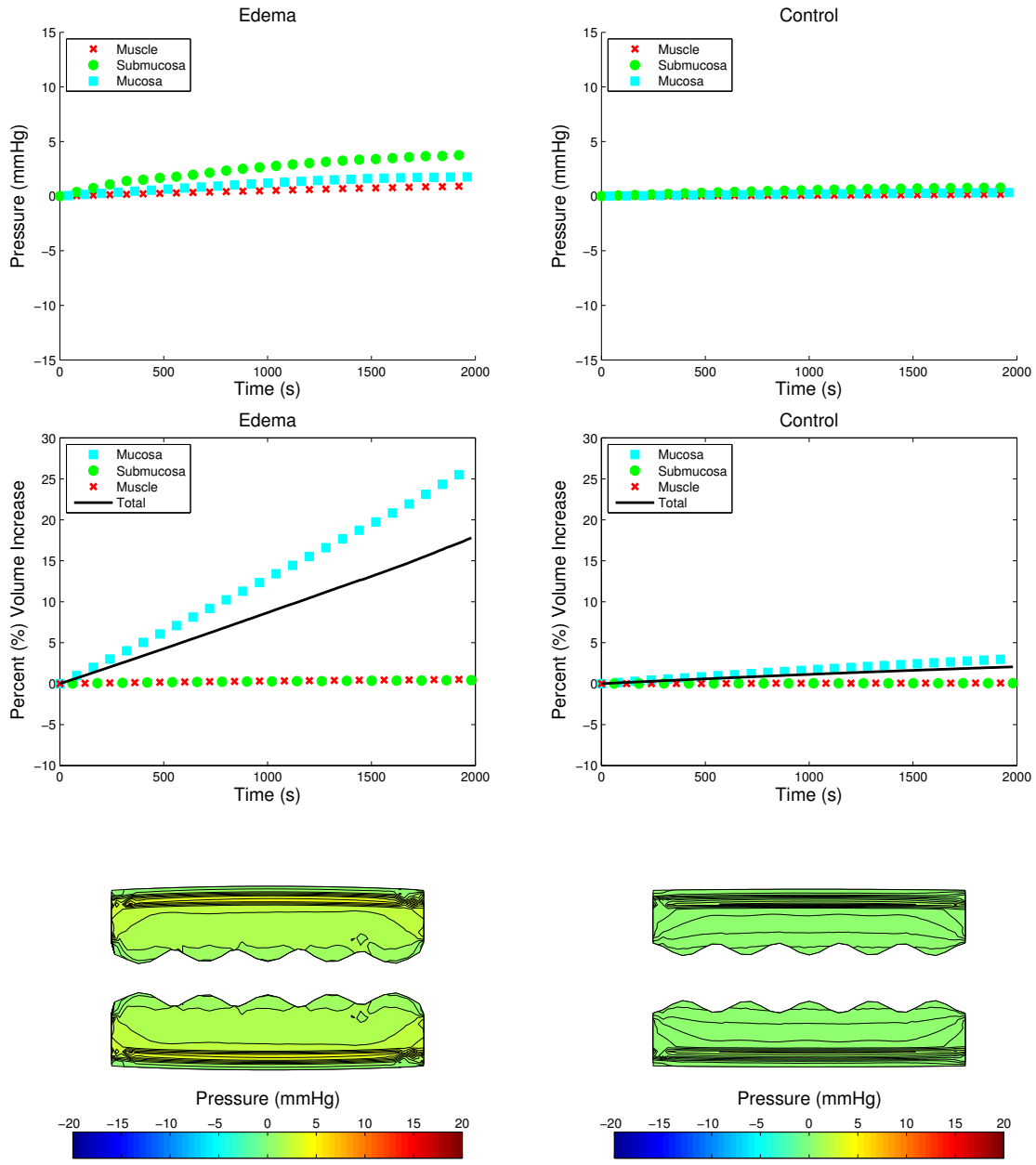


**Figure 6 Top Row: Average interstitial pressure versus time for the three subdomains, for the edema and control case simulations utilizing varying elastic moduli and a non-uniform capillary distribution. Middle Row: Percent volume increase versus time for the three subdomains and their total, for the edema and control case simulations. Bottom Row: Contour plots of the pressure at the end of the edema and control case simulations.**

**Table 2 Comparison of edema simulation results to experimental data. An * indicates this simulation did not complete all time steps.**

| | Final Submucosa $p$ | Percent Volume Increase |
|---|---|---|
| Experiment | $3.8 \pm 0.34$ mmHg | $19.8\% \pm 5\%$ |
| Avg. Moduli, Uniform $\theta(x, y) = 0.3414$ | 9.2 mmHg | -10% |
| *Avg. Moduli, Varying $\theta(x, y)$ | -2.5 mmHg | 3.7% |
| *Varying Moduli, Uniform $\theta(x, y) = 0.3414$ | -4.6 mmHg | 6.2% |
| Varying Moduli, Uniform $\theta(x, y) = 0.0059$ | 4.41 mmHg | 0.65% |
| Varying Moduli, Varying $\theta(x, y)$ | 3.79 mmHg | 17.8% |

## Varying Elasticity Moduli and Non-Uniform Capillary Distribution

The first four models, which employed various simplifications, were not able to simulate both the correct pressure and correct percent volume increase observed experimentally. In this final test, we utilize both the biologically-correct elasticity moduli and non-uniform capillary distribution function. The average, final interstitial pressure in the submucosa was found to be 3.79 mmHg and the overall percent volume increase was 17.8%. These simulation results are very similar to the experimental data. We then utilized this model to run a simulation mimicking the control group scenario from the experiments. For this case, $P_V$ was lowered to a homeostatic level of 12 mmHg. In [5], the control group's final submucosal pressure was measured to be $0.88 \pm 0.13$ mmHg, and our simulation produced a final submucosa pressure of 0.78 mmHg. The results of these two simulations are shown in Figure 6. There is a steady (but different rate) increase in pressure and volume in each layer. The mucosa has a higher concentration of capillaries and also has the lowest elastic modulus of the three layers, therefore it is intuitive that the mucosa will have the highest volume increase. The submucosa has the highest elasticity modulus and therefore will be the most resistant to deformation, which in turn causes the pressure in this layer to build up at a faster rate than in the mucosa or muscle layer.

## Conclusions

A summary of all edema simulation results compared to the edema experimental data is shown in Table 3. None of the four simplified models were able to produce both submucosal pressure values and percent volume increase values that matched the experimental data. Only the most complex model that included the spatial variation in both the mechanical parameters and the capillary concentration produced results very similar to the measured experimental values. This final model was also utilized to simulate the control case of the experiments, and these results also matched well with the measured data of [5].

Assuming a material is homogeneous in its elastic properties and structure often decreases code development time and saves computational time during simulations. However, such assumptions often limit a model's ability to realistically simulate the target phenomenon. This was the case with our simplified models of intestinal edema. The improvement in accuracy of the final model over the four simplified models was vast, providing justification for this model's complexity.

With this detailed model validated, it will be utilized in future work to explore possible links between edema development and decreased intestinal smooth muscle contractility and also to simulate the effects of various edema treatment methods.

## Acknowledgements

The first author acknowledges the support of NSF grant DMS 0739420.

## References

[1 ] R. M. Dongaonkar, C. M. Quick, R. H. Stewart, R. E. Drake, C. S. Cox, Jr., and G. A. Laine, Edemagenic gain and interstitial fluid volume regulation, *Ann. J. Physiol. Regul. Integr. Comp. Physiol.* **294**, pp. 651-659 (2008)

[2 ] R. K. Reed, Interstitial fluid pressure, In Interstitium, Connective Tissue and Lymphatics: Proceedings of the XXXII Congress of the International Union of Physiological Sciences, R. K. Reed, N. G. McHale, J. L. Bert, C. P. Winlove, and G. A. Laine, editors. *Portland Press Ltd.*, London, pp. 85-100 (1995)

[3 ] A. C. Guyton. Interrelationships among interstitial fluid volume, interstitial fluid pressure, intersitial fluid protein concentration and lymph flow, In Interstitium, Connective Tissue and Lymphatics: Proceedings of the XXXII Congress of the International Union of Physiological Sciences, R. K. Reed, N. G. McHale, J. L. Bert, C. P. Winlove, and G. A. Laine, editors, *Portland Press Ltd.*, London, pp. 167-180 (1995)

[4 ] D. N. Granger, J. Barrowman, Gastrointestinal and liver edema, In Edema, N. C. Staub, A. E. Taylor, editors, *Raven Press*, New York, pp. 615-656 (1984)

[5 ] C. S. Cox Jr., R. Radhakrishnan, L. Vilarubia, H. Xue, K. Uray, B. Gill, R. Stewart, and G. Laine, Hypertonic saline modulation of intestinal tissue stress and fluid balance, *Shock*, **29**, pp. 598-602 (2008)

[6 ] R. Radhakrishnan, H. Xue, N. Weisbrodt, F. A. Moore, S. J. Allen, G. A. Laine, and C. S. Cox Jr., Resuscitation-induced intestinal edema decreases the

stiffness and residual stress of the intestine. *Shock*, **24** pp. 165-170 (2005)

[7 ] S. D. Moore-Olufemi, H. Xue, S. J. Allen, F. A. Moore, R. H. Stewart, G. A. Laine, and C. S. Cox Jr., Inhibition of intestinal transit by resuscitation inducted gut edema is reversed by L-NIL, *J. Surg. Res.*, **129** pp. 1-5 (2005)

[8 ] S. D. Moore-Olufemi, J. Padalecki, S. E. Olufemi, H. Xue, D. H. Oliver, R. S. Radhakrishnan, S. J. Allen, F. A. Moore, R. Stewart, G. A. Laine, and C. S. Cox Jr., Intestinal edema: effect of enteral feeding on motility and gene expression. *J. Surg. Res.*, **155**, pp. 283-292 (2009)

[9 ] B. Robertson-Dunn, D. A. Linkens, A mathematical model of the slow wave electrical activity of the human small intestine, *Med. Biol. Eng.*, **12**, pp. 750-758 (1974)

[10 ] S. Metry, P. A. Arhan, and G. Chauvet, A mathematical analysis of intestinal peristaltic waves, *Med. Eng. Phys.* **17**, pp. 204-214 (1995)

[11 ] L. Francea, J. Lenoirb, A. Angelidisc, P. Meseureb, M.-P. Canic, F. Faurec, and C. Chailloub, A layered model of a virtual human intestine for surgery simulation, *Med. Image Anal.* **9** pp. 123-132 (205)

[12 ] F. R. Johnson. The digestive system. In Cunningham's Textbook of Anatomy. $12^{th}$ edition, G. J. Romanes, editor, *Oxford University Press*, Oxford, pp. 411-489 (1981)

[13 ] D. B. Wilson and W. J. Wilson. Human Anatomy, $2^{nd}$ edition, *Oxford University Press*, New York (1983)

[14 ] H. Gregersen, Biomechanics of the Gastrointestinal Tract, *Springer-Verlag*, London (2003)

[15 ] Y. Dou, J. Zhao, and H. Gregersen, Morphology and stress-strain properties along the small intestine in the rat. *J. Biomech. Eng.* **125** pp. 266-273 (2003)

[16 ] S. D. Moore-Olufemi, H. Xue, S. J. Allen, F. A. Moore, R. H. Stewart, G. A. Laine, and C. S. Cox Jr., Effects of primary and secondary intra-abdominal hypertension on mesenteric lymph flow: implications for the abdominal compartment syndrome, *Shock*, **23** pp. 571-575 (2005)

[17 ] K. S. Uray, G. A. Laine, H. Xue, S. J. Allen, and C. S. Cox Jr., Intestinal edema decreases intestinal contractile activity via decreased myosin light chain phosphorylation, *Crit. Care Med.*, **34**, pp. 2630-2637 (2006)

[18 ] K. S. Uray, G. A. Laine, H. Xue, S. J. Allen, and C. S. Cox Jr., Edema-induced intestinal dysfunction is mediated by STAT3 activation, *Shock*, **28**, pp. 239-244 (2007)

[19 ] K. S. Uray, Z. Wright, K. Kislitsyna, H. Xue, C.S . Cox Jr., Nuclear factor-$\kappa$B activation by edema inhibits intestinal contractile activity, *Crit. Care Med.*, **38**, pp. 861-870 (2010)

[20 ] M. A. Biot, General theory of three-dimensional consolidation, *J. Appl. Phys.*, **12**, pp. 155-164 (1941)

[21 ] M. A. Biot, Theory of elasticity and consolidation for a porous anisotropic solid, *J. Appl. Phys.*, **26**, pp. 182-185 (1955)

[22 ] J. Bear, Y. Bachmat, Introduction to modeling of transport phenomena in porous media. *Kluwer Academic Publishers*, Dordrecht, (1990)

[23 ] J. Young, B. Rivière, C. Cox Jr. and K. Uray, A poroelastic model of intestinal edema, *In preparation*

[24 ] M. W. Beatty, A. K. Ojha, J. L. Cook, L. R. Alberts, G. K. Mahanna, L. R. Iwasaki and J. C. Nickel, Small intestinal submucosa versus salt-extracted Polyglycolic Acid-Poly-L-lactic Acid: A comparison of neocartilage formed in two scaffold materials, *Tissue Eng.* **8**, pp. 955-968 (2002)

[25 ] A. M. Collinsworth, S. Zhang, W. E. Kraus, and G. A. Truskey, Apparent elastic modulus and hysteresis of skeletal muscle cells throughout differentiation, *Am. J. Physiol.-Cell Ph.*, **283**, pp. C1219-C1227 (2002)

[26 ] B. M. Rivière, Discontinuous Galerkin Methods for Solving Elliptic and Parabolic Equations: Theory and Implementation. *SIAM*, Philadelphia, (2008)

[27 ] B. M. Rivière, M. F. Wheeler, and V. Girault, Improved energy estimates for interior penalty, constrained and discontinuous Galerkin methods for elliptic problems. Part I, *Computat. Geosci.*, **3**, pp. 337-360 (1999)

[28 ] S. Balay, J. Brown, K. Buschelman, W. D. Gropp, D. Kaushik, M. G. Knepley, L. C. McInnes, B. F. Smith and H. Zhang, PETSc Web page. *http://www.mcs.anl.gov/petsc* (2011)

[29 ] S. Balay, J. Brown, K. Buschelman, V. Eijkhout, W. D. Gropp, D. Kaushik, M. G. Knepley, L. C. McInnes, B. F. Smith and H. Zhang, PETSc Users Manual: ANL-95/11 - Revision 3.1. Argonne National Laboratory (2010)

[30 ] S. Balay, W. D. Gropp, L. McInnes, and B. F. Smith, Efficient Management of Parallelism in Object Oriented Numerical Software Libraries in Modern Software Tools in Scientific Computing, E. Arge, A. M. Bruaset, and H. P. Langtangen, editors, *Birkhäuser Press* pp. 163-202 (1997)

[31 ] A. C. Guyton, J. E. Guyton, Textbook on Medical Physiology, $10^{th}$ edition, *Elsevier*, Philadelphia (2000)